Applied Surface Science 669 (2024) 160331

Contents lists available at ScienceDirect

Applied Surface Science

journal homepage: www.elsevier.com/locate/apsusc

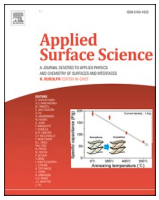

Full Length Article

Unravelling chemical etchant influences during assisted wet-transfer to obtain high quality MoS_2 atomic layers

Animesh Pratap Singh [a,1], Han Xu [a,1], Amir Ghiami [b], Songyao Tang [b], Zhaodong Wang [c], Holger Kalisch [b], Susanne Hoffmann-Eifert [c], Alwin Daus [d], Sven Ingebrandt [a], Andrei Vescan [b], Vivek Pachauri [a,*]

[a] Institute of Materials in Electrical Engineering 1, RWTH Aachen University, Sommerfeldstrasse 24, 52074 Aachen, Germany
[b] Compound Semiconductor Technology, RWTH Aachen University, Sommerfeldstrasse 18, 52074 Aachen, Germany
[c] Peter Grünberg Institut (PGI), Elektronische Materialien (PGI-7), Forschungszentrum Jülich GmbH, Wilhelm-Johnen-Straße, 52428 Jülich, Germany
[d] Sensors Laboratory, Department of Microsystems Engineering, University of Freiburg, Georges-Köhler-Allee 103, 79110 Freiburg, Germany

ARTICLE INFO

Keywords:
Transition metal dichalcogenide
Substrate transfer
KOH
2D materials
Raman spectroscopy

ABSTRACT

Two-dimensional (2D) MoS_2 is an emerging alternative to traditional semiconductors, overcoming scaling limits in device fabrication. Ongoing efforts to realize the full potential of 2D MoS_2 in CMOS back-end-of-line integration encounters notable challenges due to synthesis of such 2D materials requiring high temperature growth substrates and a transfer step. Consequently, lattice preservation of MoS_2 atomic layers during transfer from growth substrate to a target substrate is crucial for fabrication and system integration. This work, investigates the impact of commonly used chemical etchant potassium hydroxide (KOH) on MoS_2 during the poly(methyl-methacrylate) (PMMA) assisted wet-transfer process from sapphire substrates. A systematic experimental framework involving Raman spectroscopy, Atomic Force Microscopy (AFM), Optical Microscopy, and X-ray Photoelectron Spectroscopy (XPS) was employed for comparative evaluation of MoS_2 upon transfer. While the investigations highlight the relation of etchant concentration and exposure time to be the deterministic factors, topographic and spectroscopic evidence corroborate the role of K^+ ions in etching and oxidation of MoS_2 at higher concentrations affecting the MoS_2 quality. Thorough characterizations of transfer process, while following the MoS_2 quality in this work, provides crucial information on etchant concentration selection to achieve shorter substrate transfer time with minimal impact on material quality.

1. Introduction

Two-dimensional materials, such as graphene and transition metal dichalcogenides (TMDCs), hold immense potential for future technologies due to their exceptional material properties at atomic scale [1]. Graphene, as the first 2D material, exhibits outstanding thermal and electrical conductivity [2] but lacks a band gap, making it unsuitable for digital electronics [3,4]. TMDCs, such as MoS_2, offer tunable band gap [4] but typically require high-temperature growth (600–900 °C) [5–8] and specific substrates like sapphire [9 10] for good crystallinity with uniform coverage. Although, there are various reported research works showing growth of good quality MoS_2 at low synthesis temperature (200–400 °C) [11–13], there is a lack of detailed studies on high device performance with large-scale integration capability. Very recently, Xia and group produced a uniform monolayer MoS_2 coverage on 12-inch sapphire wafer [8]. Top gated transistors shows high electron mobility of 40.65 $cm^2V^{-1}s$-1 and on–off ratio of 10^8. Still, synthesis temperature is 700 °C and growth substrate is sapphire. Other work from Zhu et al. in 2023 presents synthesis of monolayer MoS_2 at growth temperature less than 300 °C on 200 mm SiO_2/Si wafers. Back-gated transistors exhibit an electron mobility of ~ 35.9 $cm^2V^{-1}s^{-1}$ [14,15]. Although growth high quality 2D MoS_2 at low temperature is advancing very fast, there are still significant challenges for low-temperature growth of other 2D materials. This limits the back-end-of-line (BEOL) integration of 2D materials into existing complementary metal oxide semiconductor (CMOS) technology to exploit their full potential [16]. One alternative is to transfer as synthesized high quality 2D material from the growth substrate to a target substrate with minimal damage to material quality, involving dry

* Corresponding author.
E-mail address: pachauri@iwe1.rwth-aachen.de (V. Pachauri).
[1] Author contributed equally.

https://doi.org/10.1016/j.apsusc.2024.160331
Received 14 March 2024; Received in revised form 10 May 2024; Accepted 18 May 2024
Available online 27 May 2024

and wet transfer methods [17,18]. polymethyl methacrylate (PMMA) assisted wet transfer, a well-established method, is used for scalable and reproducible transfer of 2D materials like graphene [19], MoS_2 [20] and hBN [21]. In the case of MoS_2, grown on sapphire due to a small lattice mismatch, etchants like sodium hydroxide (NaOH), potassium hydroxide (KOH), or buffer oxide etchant (BOE) are used to delaminate the PMMA/MoS_2 layer from the substrate. Several research works used KOH concentration of 1 M [22–24] or 2 M for the transfer process without a proper explanation of suitable KOH concentration for the transfer. Despite concerns about etchants potentially damaging MoS_2 quality, there is a lack of comprehensive studies on the effects of etchants on MoS_2 material, including physical and chemical changes.

This study carried out a systematic analysis of PMMA-assisted wet transfer of MoS_2 grown on sapphire to SiO_2/Si substrate using KOH as an etchant. The influence of KOH by varying concentration (0.2–10 M) on transfer duration and film quality was investigated and we found out that KOH concentration plays a crucial role in determining the transfer duration as well as film quality. Transfer duration decreased significantly as KOH concentration increased from 0.2 M to 5 M, while preserving film quality. At higher KOH concentrations (7 M and 10 M), transfer duration remained similar, but etching of MoS_2 as well as significant presence of MoO_x was observed. Thus, an optimal KOH concentration between the ranges 2 to 5 M was found to be suitable for a faster transfer process with minimal damage to film quality. This study provides valuable guidance for researchers working with 2D materials, highlighting the importance of optimizing transfer processes and understanding the effects of etchants on material quality.

2. Materials and methods

2.1. Substrate transfer of MoS_2 atomic layers

MoS_2 was grown by metal organic chemical vapor deposition (MOCVD) process on c-plane sapphire [25]. A 950 A6 PMMA (900–1500 k g/mol molecular weight) support layer, purchased from Micro Resist Technology GmbH in Germany, was used for the transfer processes. PMMA was spin-coated onto a 2-inch MoS_2/sapphire wafer at a speed of 3000 revolutions per minute (rpm). This step ensures uniform coverage of the PMMA layer on top of MoS_2 grown on sapphire. The PMMA-coated wafers were subsequently baked at 120 °C for 10 min to

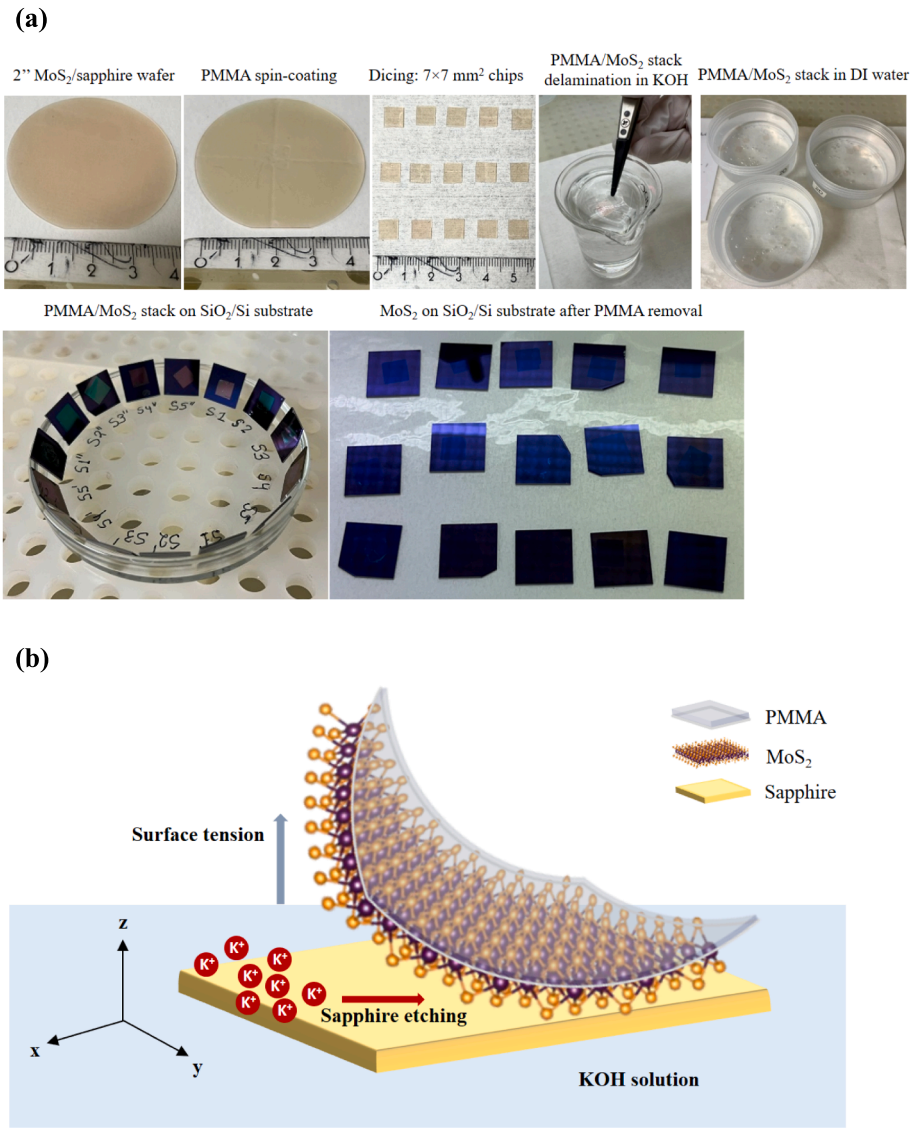

Fig. 1. Illustration showing PMMA assisted wet-transfer process of MoS_2. (a) Optical images of process steps involved in the transfer process of MoS_2 grown on 2″ sapphire substrate transferred to SiO_2/Si substrate (b) Schematic illustration of the PMMA/MoS_2 layer stack delamination from sapphire where surface tension and etching of substrate in KOH contribute to the weakening of van der Waals interactions between sapphire and MoS_2 layers.

solidify the PMMA layer and prepare it for the wet-transfer process. After baking, the wafers were allowed to cool down at room temperature for approximately 3 min. This cooling phase ensures that the PMMA layer is stable and ready for the subsequent process steps. The wafer was diced into 7 × 7 mm^2 samples (Fig. 1**a**). Aqueous Potassium hydroxide (KOH) (Carl Roth GmbH) solutions with varying concentrations (0.2 M, 2.0 M, 5.0 M, 7.0 M, and 10.0 M) were used for chemical etching and delamination of the PMMA/MoS_2 layer stack from the sapphire substrate. The experimental design involved studying the wet-transfer process on a minimum of 3 samples for each concentration (Fig. 1**a**), as well as for the samples overexposed to KOH for additional 30 and 60 min for the wet-transfer.

It is observed that the delamination process of the PMMA/MoS_2 layer stack always initiates from the edges of the sapphire substrate and gradually proceeded towards the central regions of the sample resulting in the detachment of the entire layer stack (Fig. 2**a**). Literature report suggests that the delamination occurs due to the weakening of Van der Waals interactions between the MoS_2 and sapphire substrate, facilitated by surface tension and substrate etching effects (Fig. 1**b**) [18,26]. The key steps that are involved in the transfer process are illustrated in the Fig. 1**a**. After the delamination in KOH solution, the floating PMMA/MoS_2 layer stack is fished out gently and transferred to float on the surface of deionized (DI) water. This layer stack is kept in DI water for 24 h to remove any potential contamination that may have formed during the etching and delamination steps in the KOH solution. Afterwards, the PMMA/MoS_2 layer stack are fished off from DI water surface and transferred onto the target SiO_2/Si substrates. To allow easy evaporation of water trapped between substrate and layer stack, the samples are always positioned vertically inclined for 24 h. Thereafter, the samples were baked at 135 °C to further improve the adhesion between MoS_2 and SiO_2/Si substrate. Subsequently, the samples are cleaned in acetone for 40 min at 80 °C followed by dipping in isopropanol (IPA) to remove the PMMA layer, which acted as a support during the transfer process. Acetone and IPA used in cleaning process were purchased from MicroChemicals GmbH, Germany.

2.2. Post transfer thermal annealing post of MoS_2

After the transfer of MoS_2 on Si/SiO_2 substrates, samples were subjected to a thermal annealing process in order to remove residual PMMA [27,28 29,30] and other organic contaminants from transferred MoS_2 and passivate intrinsic defects [31,45]. This annealing step ensures that the transferred MoS_2 under characterization are as uncontaminated as possible. Thermal annealing process was carried out using a UniTemp RTP-150 rapid thermal processing platform providing precise control over temperature and environment. Annealing was performed in Argon

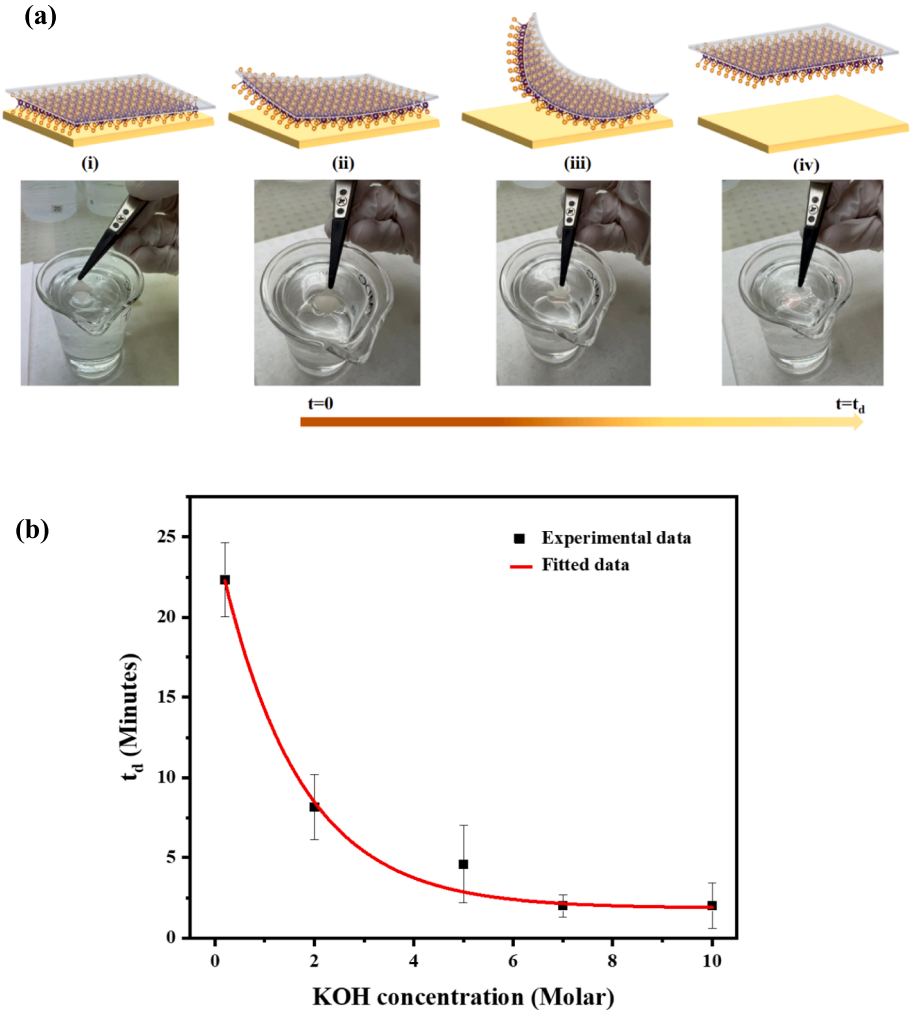

Fig. 2. Schematic illustration of delamination process characterized for the PMMA/MoS_2 layer stack from the sapphire growth substrate in this work. (a) Illustrations and optical images show the different stages of the delamination when it initiates from an edge (ii) after placing the sample in KOH solution defined as $t = 0$. Delamination proceeds slowly (iii) and finally whole film is delaminated and detached defined as $t = t_d$. (iv) (b) Graph shows that the delamination time (t_d) decreases exponentially within the KOH concentration from 0.2 M to 10 M for samples s1-s5 respectively used for wet-transfer process in this work. Error-bar represents data for N = 9.

as an inert environment at 400 °C for 1 h. The temperature was ramped up gradually at a rate of 1 °C per second. The selected temperature is high enough to effectively remove organic residues like PMMA but not as to affect the MoS_2 or the substrate. After an hour of annealing, samples are cooled down to room temperature with a rate of 1 °C per second ensuring minimal thermal shock and strain in the material [32].

3. Results and discussion

In order to systematically study the KOH etching and its influence on the quality of the substrate-transferred MoS_2 layers, KOH concentrations 0.2 M, 2 M, 5 M, 7 M, and 10 M were employed and the time required for the transfer process was calculated. The duration for the transfer process is termed as 'delamination time' t_d and defined as the time taken for the complete delamination of the PMMA/MoS_2 layer stack from the sapphire substrate once the delamination initiated from an edge. A typical delamination process as it progresses is represented in Fig. 2**a**.

As mentioned previously, two key factors influence the delamination of the PMMA/MoS_2 layer from the sapphire substrate. When the samples are immersed in the KOH solution, the liquid's surface tension acts perpendicular to the plane of the PMMA/MoS_2 layer stack as illustrated in Fig. 1**b**. In addition, KOH solution etches away the sapphire substrate and loosen the attractive substarte-2D atomic layer VdW interaction [33 34]. Same unit square area of MoS_2/PMMA stack layers were prepared for the measurement of t_d and its dependence on the KOH concentrations. The concentration dependence of t_d is shown in the Fig. 2**b** where we can see a rapid decrease in t_d as the KOH concentration is increases. At 0.2 M KOH, the delamination process is notably slow suggesting for a very slow etch rate of sapphire, requiring approximately 20–25 min for complete delamination. The delamination process at this concentration was noticed not to yield consistently clean and reproducible results, as the layer stacks sometimes broke due to exertion of extra mechanical force to delaminate the MoS_2/PMMA **(see supplementary information S7)**.

Upon increasing the KOH concentration to 2 M and 5 M, the delamination time decreases exponentially. For higher KOH concentrations (7 M and 10 M), the delamination time did not change significantly and approaches a saturation point around of 1–2 min. Interestingly, the delamination at these high KOH concentrations consistently yielded clean and intact atomic layers, requiring no additional mechanical force for delamination. This can be attributed to the rapid etching of sapphire at higher KOH concentrations, with the surface tension being sufficiently strong to lift the layer, allowing it to float within the solution. In summary, KOH concentrations in the range of 5–10 M offer a rapid and effective method for delamination of the PMMA/MoS_2 layer stacks and wet substrate transfer.

To characterize the samples, optical microscopy was used. There was no obvious contrast difference among samples s1-s5 between MoS_2 and SiO_2 (Fig. 3). Thus, visibly there is no difference among all the samples. As an established technique to provide valuable insights into the material properties of 2D materials, Raman spectroscopy was used to characterize the MoS_2 after the wet-transfer is carried out [35]. The Raman characterization results are summarized in the Fig. 4. The graph shown in Fig. 4**a** shows typical Raman spectra recorded for the 5 samples, s1 to s5 representing PMMA assisted wet-transfer using KOH concentrations 0.2, 2.0, 5.0, 7.0 and 10.0 M of KOH solutions respectively. Two distinct Raman peaks at 384 and 407 cm^{-1} can be observed for all the MoS_2 samples (s1 to s5), which correspond to the E^1_{2g} and A_{1g} vibrational modes of MoS_2 crystal lattice. The wave number difference of the peaks A_{1g} and E^1_{2g} for sample s1 (0.2 M KOH as etchant) is approximately 23.8 cm^{-1} suggesting the transferred MoS_2 to be 4 to 5 atomic layers thick, in line with previous findings [4]. What is noticeable from the graph shown in Fig. 4**b** is a consistent trend of slight decrease in this peak difference across the all the samples (s1 to s5 and five points on each sample) that are measured. The sample s5 exhibits a blue-shift in the E^1_{2g} mode and redshift for the A_{1g} vibrational mode, resulting in a maximum peak difference measured around 23.3 cm^{-1}. A comparison of spectral peaks representing E^1_{2g} and A_{1g} modes for samples s1 to s4 in detail shows no consistent trend in full width at half maximum (FWHM) and the peak-intensities. For sample s5, there is a rapid increase in the FWHM (Fig. 4**c**) and decrease in the peak intensities (Fig. 4**d**) for E^1_{2g} and A_{1g} modes. These observations collectively indicate that the crystal quality of MoS_2 is adversely affected following the transfer process with 10 M KOH. The most likely reason for polycrystalline characteristics of the transferred layers are the induction of lattice defects caused by the oxidation and dissolution of MoS_2 in a base solution [36]. The reaction mechanism can be shown as follows:

$$xK + MoS_2 \rightarrow K_xMoS_2 \quad (1)$$

$$K_xMoS_2 + yK^+ \rightarrow K_2S + Mo \quad (2)$$

$$MoS_2 + \frac{9}{2}O_2 + 3H_2O \rightarrow MoO_4^{2-} + 2SO_4^{2-} + 6H^+ \quad (3)$$

The above-mentioned study on oxidation and dissolution of MoS_2 was conducted using 1 M PBS (approximately 0.2 M Na^+ and K^+ ions) over

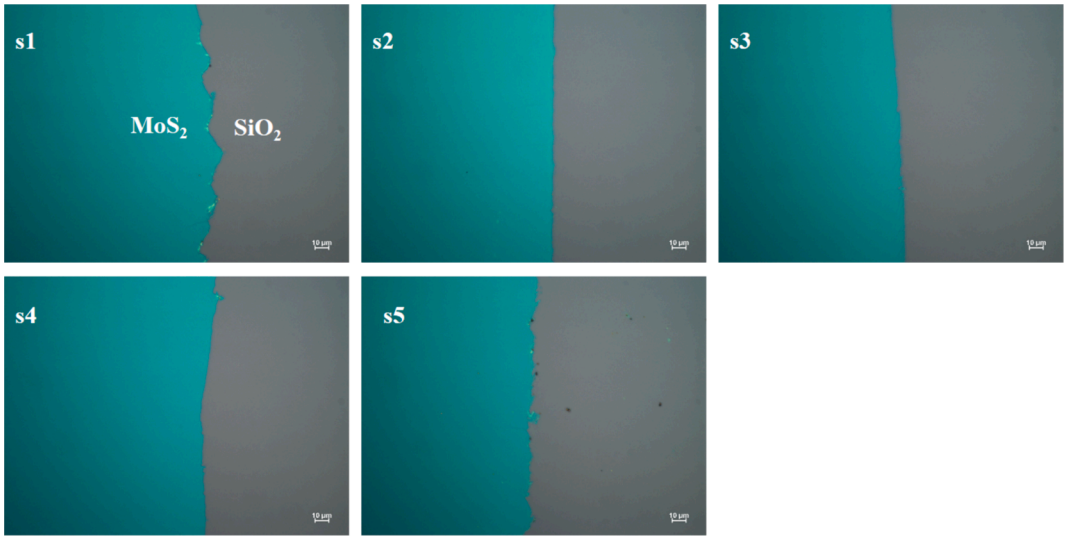

Fig. 3. Optical images of MoS_2 samples (s1-s5) after transfer using different KOH concentration (0.2, 2, 5, 7, 10 M). There is no noticeable difference in color contrast of MoS_2 across samples s1-s5. Scale-bar length in the images is 10 μm.

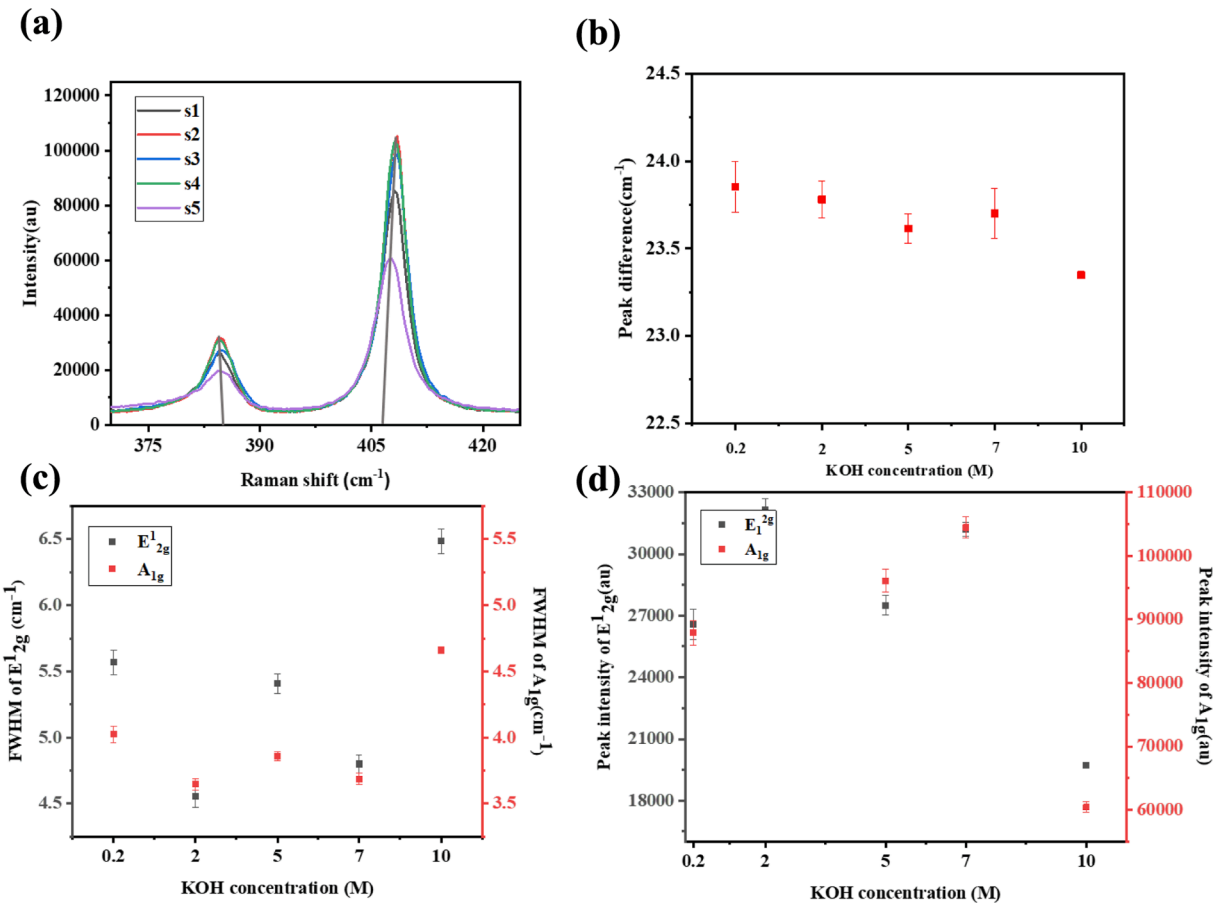

Fig. 4. Raman characterization of MoS_2 after wet-transfer using different concentrations of KOH. (a) An overview of Raman spectra showing representative Raman modes (E^1_{2g} around 383 cm^{-1} and A_{1g} around 407 cm^{-1}) for samples s1to s5. Two vertical lines shows the shift of E^1_{2g} (blue shift) and A_{1g} (red shift). (b) Variation of peak difference in Raman modes against different etchant concentrations, (c) changes in FWHM of the representative Raman modes, and (d) change in the Raman peak intensities for E^1_{2g} and A_{1g} modes against the KOH concentrations. Error-bar represents data for N = 15. (For interpretation of the references to color in this figure legend, the reader is referred to the web version of this article.)

several days to observe the degradation, it is reasonable to anticipate similar effects with significantly higher concentrations in shorter durations of exposure. Additionally, KOH is known to etch and dissolve MoO_3 via formation of a complex metal salt K_2MoO_4, resulting in the formation of lattice defects [37]. Such lattice defects alter the intensity of Raman vibrational modes due to changes in optical interference. It is important to note of several studies that have demonstrated the oxidation of MoS_2 occurring primarily at defect sites such as point defects, edge sites, and grain boundaries [38,39]. These two mechanisms are likely to have affected the crystallinity of the MoS_2 atomic layers that were substrate transferred using high 10 M KOH concentration.

In order to see the influences of etchant concentrations on the topography of atomic layers, atomic force microscopy (AFM) characterizations were carried out on as grown and transferred MoS_2. The topography characterization outcomes are summarized in supporting information **S2** (as grown MoS_2 on sapphire) and Fig. 5 (after transfer). MoS_2 grown on sapphire substrate and post annealing at 400 °C exhibit surface roughness in the range of 1 to 2 nm (**Figure S2**). Such roughness values are a result of the MOCVD growth process that is optimized in-house for wafer-scale growth of mono to few-layer MoS_2 and inadvertently includes nano-islands, which is termed as 'parasitic nucleation' on the top MoS_2 layer (Fig. 5**a**) [25,40]. As shown in the AFM scan and height profile of Fig. 5**a**, the average thickness of MoS_2 grown over 2″ wafer transferred to SiO_2/Si substrate is around 3–4 nm. The triangular nanoscale islands can be identified in the AFM scan images as well as scanning electron microscopy (SEM) images throughout (**also see supplementary information S2**). An increase in roughness is typically attributed to several factors, including residual polymer (e.g. PMMA) residues and the presence of other heterogeneities, such as tearing and folds of atomic layers on the surface. While it is challenging to completely remove such influences on the topography, [41] cleaning steps post-transfer were carefully implemented as discussed in the section 2 above in order to analyze the etchant influence on the topography. Fig. 5**b** from images (i-v) show typical AFM scans associated with the samples s1 to s5. The mean roughness (S_a) and RMS roughness (S_q) values from such representative AFM scans for samples s1 to s5 at five different points are marked in graph (Fig. 5**c**), where it shows an increasing trend from samples s1 to sample s4 while decreased significantly for sample s5 associated with the use of 10 M KOH as an etchant. This unique condition for s5 can be explained by the etching of monolayer nano-islands on top of MoS_2 layers, which are known to contribute significantly to the overall roughness.

Considering that the etching time may also directly influence the topography of the transferred MoS_2, an additional study was carried out wherein the atomic layers were allowed to remain in the KOH solutions for additional periods of 30 min (s1′to s5′) and 60 min (s1′'to s5′') after the complete delamination. The influence of this additional etching time on MoS_2 layers was clearly visible for samples s5′ and s5′' and therefore also characterized using optical microscopy (**see supplementary information S3**). The contrast between transferred MoS_2 layer and Si/SiO_2 substrate is significantly reduced for samples s5′ and s5′' along with non-uniform coverage. Raman characterizations of samples s1′- s5′ and s1′'-s5′' exhibit characteristic Raman peaks for both vibrational modes, however with peak intensities significantly reduced in comparison to

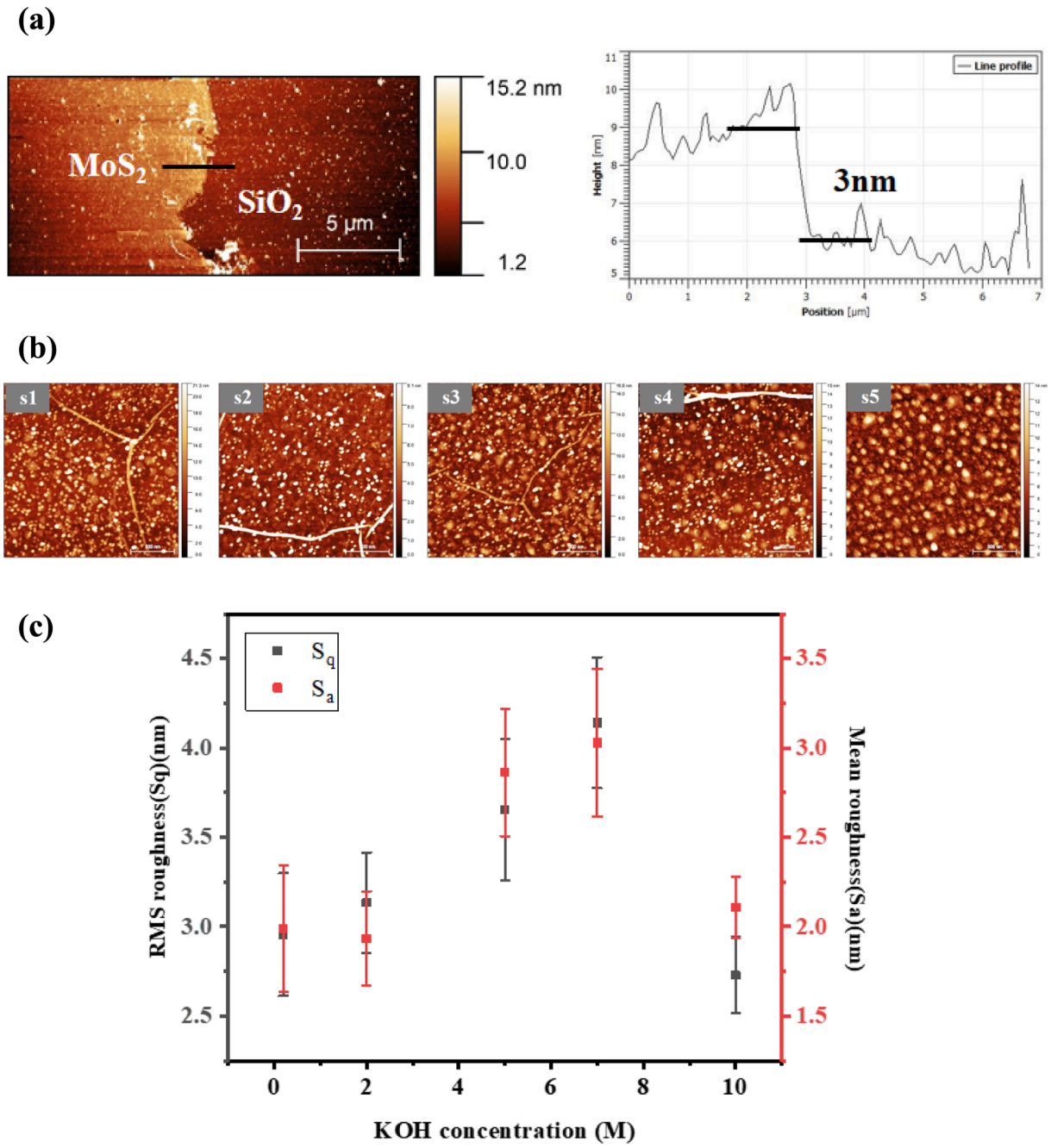

Fig. 5. Surface characterization of substrate transferred MoS_2 atomic layers using atomic force microscopy. (a) AFM scan image of a typical substrate transferred MoS_2 atomic layer on SiO_2 substrate carried out at its edge along the black-line shows topography and height profile, measuring the thickness of transferred layer at 2.7 ± 0.3 nm. (b) AFM scan images (i-v) represent MoS_2 layers substrate transferred using 0.2, 2.0, 5.0, 7.0 and 10.0 M KOH solutions denoted as samples s1to s5. (c) The graph shows the surface roughness of MoS_2 atomic layers samples at their respective t_d. Error-bar represents data for N = 15.

sample s5 (figure S4). Comparison of AFM and Raman characteristics clearly indicates that the quality of MoS_2 is affected after exposure to KOH for longer times or for high concentration. Surface roughness characterizations for the samples s5′ and s5′′ weren't considered for their very high non-uniformity (figure S3). The topographic comparison of MoS_2 atomic layers subjected to prolonged substrate etching is given in supplementary information (**S5**) where the surface roughness increases from sample s1′ to s3′ and then decreases for s4′ with values comparable to s1′. On the other hand, the surface roughness for samples s1′′ to s4′′ (60 min over exposure) show a decreasing trend. An overarching comparison of these etching conditions and resulting surface roughness indicate the use of KOH concentration above 7 M and prolonged exposure to such high concentrations associated with decrease of R_a and R_{rms} values. Monolayer MoS_2 nano-islands being a major contributor to the surface roughness apart from the polymeric residues, anisotropic etching of MoS_2 towards the removal of nanoscale islands seems to be the main occurring phenomenon here, which requires further proof.

Therefore, to collect evidence for the proposed chemical processes upon exposure to KOH and resulting roughness, high-resolution X-ray photoelectron spectroscopy (XPS) was carried out for samples s1 to s5. The XPS spectra recorded for all the samples show characteristic Mo 3d energy peaks around 230 eV and 233 eV (Fig. 6**a**) and S 2p peak around 162 eV (Fig. 6**c**). The peaks at binding energies 230 eV and 233 eV are attributed to the $3d_{5/2}$ and $3d_{3/2}$ orbitals of Mo in MoS_2 confirming the presence of MoS_2 in all the samples [42,43]. There are, however, notable variations in Mo 3d spectra of the MoS_2 layers with the appearance of an

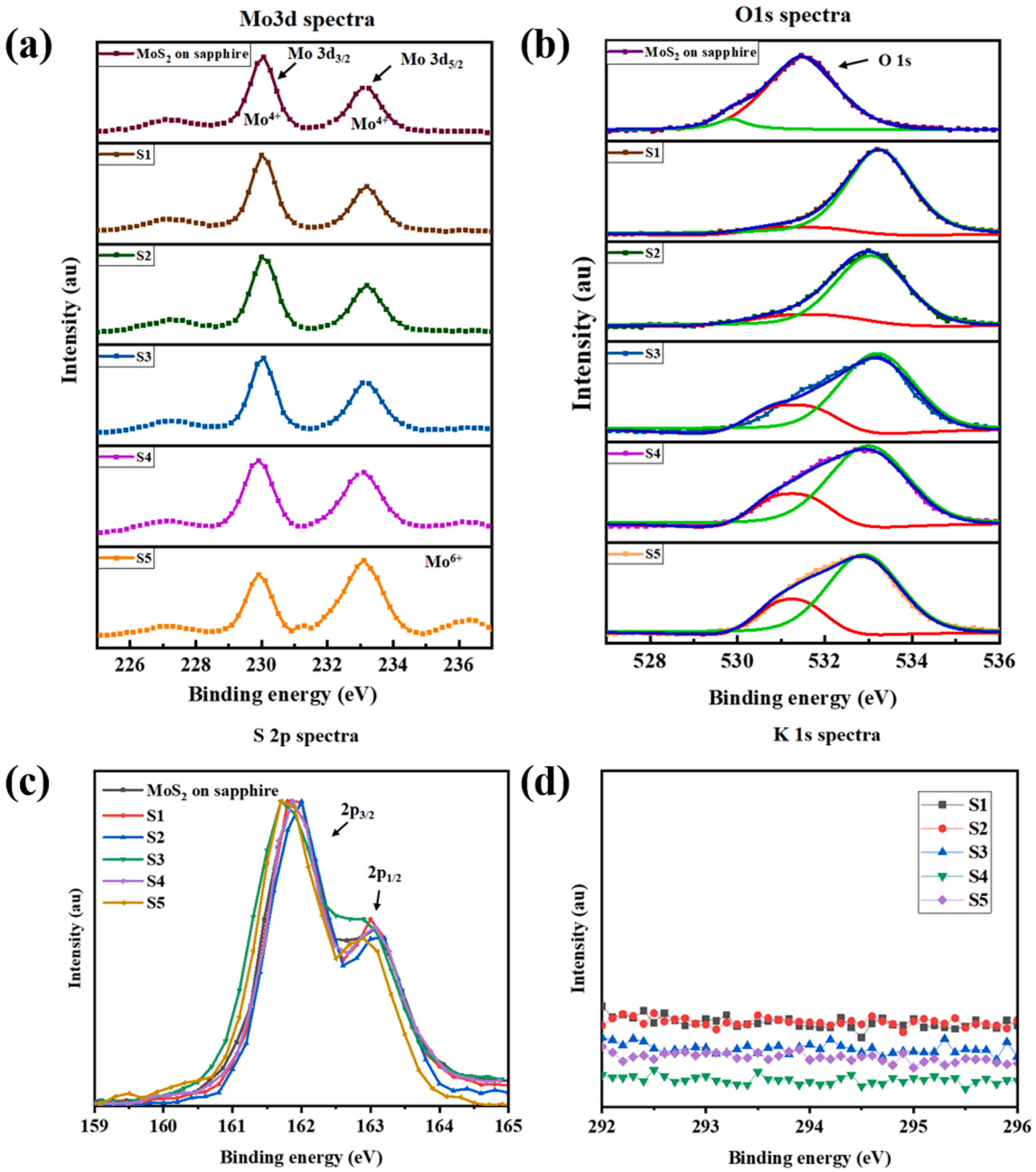

Fig. 6. X-ray photoelectron spectroscopy characterization of substrate transferred MoS_2 atomic layers with different KOH concentrations at t_d. (a) Mo 3d spectra of MoS_2 atomic layers on growth substrate (sapphire) and after wet transfer on to Si/SiO_2 substrate (s1-s5), (b) O 1 s spectra of MoS_2 atomic layers on growth substrate (sapphire) and after wet transfer on to Si/SiO_2 substrate (s1-s5). The energy peak around 531 eV corresponds to Al_2O_3 in MoS_2 on sapphire. Spectral fit of peaks around 533 eV corresponds to SiO_2 (green) whereas 531 eV corresponds to presence of MoO_2/MoO_3 in s1 to s5 on Si/SiO_2 substrate. The MoS_2 layers s3, s4, s5 start to show the presence of oxide. (c) S 2p spectra shows the presence of MoS_2 in all the samples without any other sulfur containing entities. (d) K 1 s spectra for layers s1 to s5 confirming absence of any K contamination. (e) Schematic illustration of MoS_2 etching mechanism at low/high KOH concentration/exposure time. MoS_2 nano-islands on surface of topmost monolayer can be etched away easily due to high exposure and reaction with KOH from all directions. (For interpretation of the references to color in this figure legend, the reader is referred to the web version of this article.)

additional peak at 236 eV corresponding to the binding energy of Mo in MoO_3. This peak at 236 eV becomes more pronounced for MoS_2 samples s4 and s5, which were transferred using 7 M and 10 M KOH, respectively. Such significant changes in Mo 3d spectra strongly imply the reaction of KOH with MoS_2, resulting in the formation of MoO_3. As shown in Fig. 6**b**, these chemical transformations are reflected from the energy peak around 533 eV in the O 1 s spectra corresponds to transferred layers. In sample s3, s4 and s5, the energy peak around 531 eV can be seen which corresponds to oxide entities of Mo (MoO_2, MoO_3) [44]. This peak becomes more prominent for layers s4 and s5 indicating the increase of oxide concentration with the increase in KOH concentration while transfer. It is also important to note that there is no presence of K or K^+ related energy peaks in the XPS analyses (Fig. 6**d**), suggesting no trace of K element as contamination in the transferred atomic layers.

Combining the results from spectroscopic (Raman and XPS) and microscopy (AFM) the influence of KOH as substrate etchant and its influence on the MoS_2 layers during the wet-transfer can be summarized by a descriptive of the resultant chemical processes, which are

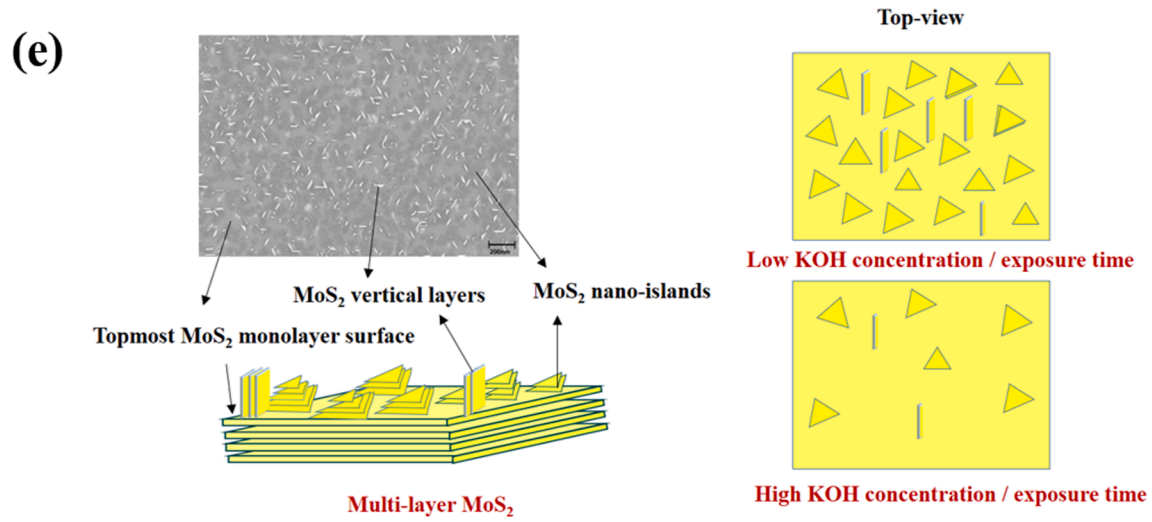

Fig. 6. (*continued*).

illustrated in Fig. 6**e.** First, the surface topography of MoS_2 layers exhibiting open lattice-edges significantly influences the etching processes, which in this study is evident from the presence of monolayer nanoscale islands that are readily etched away when exposed to high etchant concentrations. Second, the etchant (KOH) reaction to the continuous MoS_2 layers, particularly at the defects sites and edges replace the S-atoms and generation of Mo-oxides resulting in the degradation of lattice properties.

4. Conclusions and outlook

A systematic investigation into the study of chemical etchant's influence on 2D MoS_2 during the PMMA assisted wet ransfer has been presented in this work. Sapphire being the most used growth substrate for MoS_2 growth, KOH's influence on MOCVD grown MoS_2 cystal quality during the wet-transfer onto SiO_2/Si substrates is studied. Experimental characterizations of MoS_2 transferred using different KOH concentrations (from 0.2 M to 10 M) and durations were carried out using Raman spectroscopy, high-resolution XPS spectroscopy, AFM and optical microscopy. By taking same unit sqare area (7×7 mm^2) on the same sappphire growth substrate, the duration required for a full delamination of PMMA coated MoS_2 stack from the substrate in KOH was characterized as t_d. The t_d displays a notable trend of decreasing exponentially with an increase in KOH concentration without affecting the quality of transfer process upto a certain extent. At low KOH concentration (0.2 M), delamination of MoS_2 is cumbersome as the transfer process lacks reproducibility due to slowed down chemical processes. Conversely, high KOH concentrations (5 M-10 M) have a significant impact on the transfer process where resulting quality is highly dependent on the topography of as grown MoS_2 layers. MoS_2 layers with more of such nano-islands or vertically oriented layers, an elevated concentration of K^+ ions can not only etch and dissolve MoS_2 but also results in formation of substantial amont of oxide (MoO_3). This study pinpoints an optimal range for KOH concentration, from 2 to 5 M, as a suitable choice for achieving a rapid substrate transfer process with minimal affect on MoS_2 atomic layers. These results are expected to serve as a foundation and framework to extending similar investigations on other layered materials and etchants such as NaOH, buffer oxide etchant, commonly used in the 2D materials family. It is worth mentioning that a systematic exploration of the influence of various solvents and chemicals employed in clean-room oriented nanofabrication processes towards system integration of MoS_2 and other 2D materials will pave the way towards process standardization and harnessing the potential of 2D materials with better know-how.

CRediT authorship contribution statement

Animesh Pratap Singh: Writing – original draft, Visualization, Validation, Software, Methodology, Investigation, Formal analysis, Data curation. **Han Xu:** Writing – original draft, Visualization, Investigation, Data curation. **Amir Ghiami:** Writing – review & editing, Resources, Investigation. **Songyao Tang:** Writing – review & editing, Resources, Investigation. **Zhaodong Wang:** Writing – review & editing, Validation, Investigation, Data curation. **Holger Kalisch:** Writing – review & editing, Resources. **Susanne Hoffmann-Eifert:** Visualization, Supervision, Investigation. **Alwin Daus:** Writing – review & editing, Methodology. **Sven Ingebrandt:** Writing – review & editing, Resources, Project administration. **Andrei Vescan:** Writing – review & editing, Supervision, Resources. **Vivek Pachauri:** Writing – review & editing, Writing – original draft, Supervision, Resources, Project administration, Methodology, Investigation, Funding acquisition, Conceptualization.

Declaration of competing interest

The authors declare that they have no known competing financial interests or personal relationships that could have appeared to influence the work reported in this paper.

Data availability

Data will be made available on request.

The data that support the findings of this study are available upon reasonable request from the authors

Acknowledgements

We gratefully acknowledge the financial support from DFG project BioNanoLock (grant no. 440055779) and Federal Ministry of Education and Research (BMBF) project NEUROTEC-II, (grant no. 16ME0399). Experiments was carried out in the Central Laboratory for Micro- and Nanotechnology (CMNT) at RWTH Aachen University. Technical support by CMNT staff Mr. Jochen Heiss, Mrs. Dorothee Breuer and Mrs. Ewa-Janina Sekula is gratefully acknowledged. We thank Regina Dittmann and her team for support at the Electronic Oxide Cluster at Research Center Jülich.

Appendix A. Supplementary data

Supplementary data to this article can be found online at https://doi.

org/10.1016/j.apsusc.2024.160331.

References

[1] R. Mas-Balleste, C. Gomez-Navarro, J. Gomez-Herrero, F. Zamora, 2D materials: to graphene and beyond, Nanoscale 3 (2011) 20–30.

[2] A.H. Castro Neto, F. Guinea, N.M.R. Peres, K.S. Novoselov, A.K. Geim, The electronic properties of graphene, Rev. Mod. Phys. 81 (2009) 109–162.

[3] P. Avouris, Graphene: electronic and photonic properties and devices, Nano Lett 10 (2010) 4285–4294.

[4] C. Lee, H. Yan, L.E. Brus, T.F. Heinz, J. Hone, S. Ryu, Anomalous lattice vibrations of single- and few-layer MoS2, ACS Nano 4 (2010) 2695–2700.

[5] Z.S. Zhu, S.B. Zhan, J. Zhang, G.S. Jiang, M.F. Yi, J. Wen, Influence of growth temperature on MoS2 synthesis by chemical vapor deposition, Mater. Res. Express 6 (2019) 095011.

[6] H. Xu, H. Zhang, Z. Guo, Y. Shan, S. Wu, J. Wang, W. Hu, H. Liu, Z. Sun, C. Luo, X. Wu, Z. Xu, D.W. Zhang, W. Bao, P. Zhou, High-Performance Wafer-Scale MoS(2) Transistors toward Practical Application, Small 14 (2018) e1803465.

[7] Y. Kim, A.R. Kim, G. Zhao, S.Y. Choi, S.C. Kang, S.K. Lim, K.E. Lee, J. Park, B. H. Lee, M.G. Hahm, D.H. Kim, J. Yun, K.H. Lee, B. Cho, Wafer-Scale Integration of Highly Uniform and Scalable MoS(2) Transistors, ACS Appl Mater Interfaces 9 (2017) 37146–37153.

[8] Y. Xia, X. Chen, J. Wei, S. Wang, S. Chen, S. Wu, M. Ji, Z. Sun, Z. Xu, W. Bao, P. Zhou, 12-inch growth of uniform MoS(2) monolayer for integrated circuit manufacture, Nat Mater 22 (2023) 1324–1331.

[9] D. Dumcenco D. Ovchinnikov K. Marinov P. Lazic M. Gibertini N. Marzari O. Lopez Sanchez Y.C. Kung D. Krasnozhon M.W. Chen S. Bertolazzi P. Gillet A. Fontcuberta i Morral, A. Radenovic, A. Kis, -Area Epitaxial Monolayer MoS2 ACS Nano 9 2015 4611 4620.

[10] H. Yu, M. Liao, W. Zhao, G. Liu, X.J. Zhou, Z. Wei, X. Xu, K. Liu, Z. Hu, K. Deng, S. Zhou, J.A. Shi, L. Gu, C. Shen, T. Zhang, L. Du, L. Xie, J. Zhu, W. Chen, R. Yang, D. Shi, G. Zhang, Wafer-Scale Growth and Transfer of Highly-Oriented Monolayer MoS(2) Continuous Films, ACS Nano 11 (2017) 12001–12007.

[11] S.W. Chung, S. Ganorkar, S.I. Kim, Low-temperature synthesis of MoS2 at 200 °C, J. Korean Phys. Soc. 82 (2023) 1211–1215.

[12] J.H. Park, A.Y. Lu, P.C. Shen, B.G. Shin, H. Wang, N. Mao, R. Xu, S.J. Jung, D. Ham, K. Kern, Y. Han, J. Kong, Synthesis of High-Performance Monolayer Molybdenum Disulfide at Low Temperature, Small Methods 5 (2021) e2000720.

[13] R.M. Neubieser, J.L. Wree, J. Jagosz, M. Becher, A. Ostendorf, A. Devi, C. Bock, M. Michel, A. Grabmaier, Low-temperature ALD process development of 200 mm wafer-scale MoS2 for gas sensing application, Micro and Nano Engineering 15 (2022) 100126.

[14] J. Zhu, J.H. Park, S.A. Vitale, W. Ge, G.S. Jung, J. Wang, M. Mohamed, T. Zhang, M. Ashok, M. Xue, X. Zheng, Z. Wang, J. Hansryd, A.P. Chandrakasan, J. Kong, T. Palacios, Low-thermal-budget synthesis of monolayer molybdenum disulfide for silicon back-end-of-line integration on a 200 mm platform, Nat Nanotechnol 18 (2023) 456–463.

[15] M.C. Lemme, A. Daus, Low-temperature MoS(2) growth on CMOS wafers, Nat Nanotechnol 18 (2023) 446–447.

[16] C. Huyghebaert T. Schram Q. Smets T.K. Agarwal D. Verreck S. Brems A. Phommahaxay D. Chiappe S.E. Kazzi C.L.d.l. Rosa, G. Arutchelvan, D. Cott, J. Ludwig, A. Gaur, S. Sutar, A. Leonhardt, D. Marinov, D. Lin, M. Caymax, I. Asselberghs, G. Pourtois, I.P. Radu, 2D materials: roadmap to CMOS integration In: 2018 IEEE International Electron Devices Meeting (IEDM) 2018 pp. 22.21.21-22.21.24.

[17] T.F. Schranghamer, M. Sharma, R. Singh, S. Das, Review and comparison of layer transfer methods for two-dimensional materials for emerging applications, Chem Soc Rev 50 (2021) 11032–11054.

[18] A.J. Watson, W.B. Lu, M.H.D. Guimaraes, M. Stöhr, Transfer of large-scale two-dimensional semiconductors: challenges and developments, 2d Materials 8 (2021) 032001.

[19] G. Deokar, J. Avila, I. Razado-Colambo, J.L. Codron, C. Boyaval, E. Galopin, M. C. Asensio, D. Vignaud, Towards high quality CVD graphene growth and transfer, Carbon 89 (2015) 82–92.

[20] M. Sharma, A. Singh, R. Singh, Monolayer MoS2 Transferred on Arbitrary Substrates for Potential Use in Flexible Electronics, Acs Applied Nano Materials 3 (2020) 4445–4453.

[21] S. Fukamachi P. Solis-Fernández K. Kawahara D. Tanaka T. Otake Y.C. Lin K. Suenaga H. Ago Large-area synthesis and transfer of multilayer hexagonal boron nitride for enhanced graphene device arrays Nat. Electron. 6 (2023) 126-+.

[22] C.A. Bhuyan, K.K. Madapu, K. Prabakar, A. Das, S.R. Polaki, S.K. Sinha, S. Dhara, A Novel Methodology of Using Nonsolvent in Achieving Ultraclean Transferred Monolayer MoS2, Adv. Mater. Interfaces 9 (2022).

[23] C.A. Bhuyan, K.K. Madapu, S. Dhara, The comparative defect study on the polymeric transfer of MoS2 monolayers, arXiv preprint arXiv:2101.06996, (2021).

[24] T. Pham, Y. Chen, J. Lopez, M. Yang, T.T. Tran, A. Mulchandani, Effect of Al(2)O (3) Passive Layer on Stability and Doping of MoS(2) Field-Effect Transistor (FET) Biosensors, Biosensors (basel) 11 (2021).

[25] S.Y. Tang, A. Grundmann, H. Fiadziushkin, A. Ghiami, M. Heuken, A. Vescan, H. Kalisch, Detailed study on MOCVD of wafer-scale MoS2 monolayers: From nucleation to coalescence, MRS Adv. 7 (2022) 751–756.

[26] A. Gurarslan, Y. Yu, L. Su, Y. Yu, F. Suarez, S. Yao, Y. Zhu, M. Ozturk, Y. Zhang, L. Cao, Surface-energy-assisted perfect transfer of centimeter-scale monolayer and few-layer MoS(2) films onto arbitrary substrates, ACS Nano 8 (2014) 11522–11528.

[27] Y.C. Lin, C.C. Lu, C.H. Yeh, C. Jin, K. Suenaga, P.W. Chiu, Graphene annealing: how clean can it be? Nano Lett 12 (2012) 414–419.

[28] Y. Ahn, H. Kim, Y.H. Kim, Y. Yi, S.I. Kim, Procedure of removing polymer residues and its influences on electronic and structural characteristics of graphene, Appl. Phys. Lett. 102 (2013).

[29] K. Kumar, Y.S. Kim, E.H. Yang, The influence of thermal annealing to remove polymeric residue on the electronic doping and morphological characteristics of graphene, Carbon 65 (2013) 35–45.

[30] M. Sharma, A. Singh, P. Aggarwal, R. Singh, Large-Area Transfer of 2D TMDCs Assisted by a Water-Soluble Layer for Potential Device Applications, ACS Omega 7 (2022) 11731–11741.

[31] M.Z. Xie, J.Y. Zhou, H. Ji, Y. Ye, X. Wang, K. Jiang, L.Y. Shang, Z.G. Hu, J.H. Chu, Annealing effects on sulfur vacancies and electronic transport of MoS2 films grown by pulsed-laser deposition, Appl. Phys. Lett. 115 (2019).

[32] H.Q. Zhao, X. Mao, D. Zhou, S. Feng, X. Shi, Y. Ma, X. Wei, Y. Mao, Bandgap modulation of MoS(2) monolayer by thermal annealing and quick cooling, Nanoscale 8 (2016) 18995–19003.

[33] K.R. Williams, K. Gupta, M. Wasilik, Etch rates for micromachining processing - Part II, J. Microelectromech. Syst. 12 (2003) 761–778.

[34] Y. Shang, H. Zhang, Y. Zhang, Research on Sapphire Deep Cavity Corrosion and Mask Selection Technology, Micromachines (basel) 12 (2021) 136.

[35] R. Saito, Y. Tatsumi, S. Huang, X. Ling, M.S. Dresselhaus, Raman spectroscopy of transition metal dichalcogenides, J Phys Condens Matter 28 (2016) 353002.

[36] X. Chen, Y.J. Park, M. Kang, S.K. Kang, J. Koo, S.M. Shinde, J. Shin, S. Jeon, G. Park, Y. Yan, M.R. MacEwan, W.Z. Ray, K.M. Lee, J.A. Rogers, J.H. Ahn, CVD-grown monolayer MoS(2) in bioabsorbable electronics and biosensors, Nat Commun 9 (2018) 1690.

[37] A. Aracena, A. Sanino, O. Jerez, Dissolution kinetics of molybdite in KOH media at different temperatures, Trans. Nonferrous Met. Soc. Chin. 28 (2018) 177–185.

[38] N.S. Rajput, A. Kotbi, K. Kaja, M. Jouiad, Long-term aging of CVD grown 2D-MoS2 nanosheets in ambient environment, npj Mater. Degrad. 6 (2022) 75.

[39] H. Lamkaouane, H. Ftouhi, M. Richard-Plouet, N. Gautier, N. Stephant, M. Zazoui, M. Addou, L. Cattin, J.C. Bernede, Y. Mir, G. Louarn, Efficient and Facile Synthetic Route of MoO(3):MoS(2) Hybrid Thin Layer via Oxidative Reaction of MoS(2) Nanoflakes, Nanomaterials (basel) 12 (2022) 3171.

[40] D.S. Schneider, A. Grundmann, A. Bablich, V. Passi, S. Kataria, H. Kalisch, M. Heuken, A. Vescan, D. Neumaier, M.C. Lemme, Highly Responsive Flexible Photodetectors Based on MOVPE Grown Uniform Few-Layer MoS, ACS Photonics 7 (2020) 1388–1395.

[41] Y.P. Xiao, W.W. Zheng, B. Yuan, C. Wen, M. Lanza, Highly Accurate Thickness Determination of 2D Materials, Cryst. Res. Technol. 56 (2021) 2100056.

[42] J.T. Kowallick, A.A. Joseph, C. Unterberg-Buchwald, M. Fasshauer, K. van Wijk, K. D. Merboldt, D. Voit, J. Frahm, J. Lotz, J.M. Sohns, Real-time phase-contrast flow MRI of the ascending aorta and superior vena cava as a function of intrathoracic pressure (Valsalva manoeuvre), Br J Radiol 87 (2014) 20140401.

[43] A. Ghiami, A. Grundmann, S.Y. Tang, H. Fiadziushkin, Z.D. Wang, S. Aussen, S. Hoffmann-Eifert, M. Heuken, H. Kalisch, A. Vescan, Impact of Carbon Impurities on Air Stability of MOCVD 2D-MoS, Surfaces 6 (2023) 351–363.

[44] H. Liu, X. Chen, L. Deng, M. Ding, J. Li, X. He, Perpendicular growth of few-layered MoS2 nanosheets on MoO3 nanowires fabricated by direct anion exchange reactions for high-performance lithium-ion batteries, J. Mater. Chem. A 4 (2016) 17764–17772.

[45] M.H. Johari, M.S. Sirat, M.A. Mohamed, Y. Wakayama, A.R. Mohmad, Effects of post-annealing on MoS2 thin films synthesized by multi-step chemical vapor deposition Nanomater, Nanotechnol. 11 (2021), https://doi.org/10.1177/1847980420981537.